CHAPTER 6

Double glassy states and large spontaneous and conventional exchange bias effect in $La_{1.5}Ca_{0.5}CoFeO_6$ double perovskite

6.1 Introduction:

In recent years, the study of double perovskite (DP) oxide materials has drawn huge attention in research and technology as they exhibit numerous and alluring functional properties like, near room temperature magnetic ordering, magneto-dielectric coupling (MDC), exchange-bias effect (EB), magneto-caloric effect, magneto-resistance (MR) etc [20, 51, 288, 289]. Double perovskite oxides have a general formula $A_2BB'O_6$, where, A is rare earth or alkaline earth material, B and B′ are d- block transition metals [290]. Partial substitution of A/B- site element creates the disorderness in the structure of DP oxides, which explore the enhanced multifunctional features in such systems [291]. From technological aspects, DP oxides have plentiful areas of applications such as in spintronics, magnetic field sensor, high density recording media and infrared detectors [292-294]. The electrical and magnetic phenomena of these oxides are governed by the coupling between charge, spin, orbital, lattice degrees of freedom and site antisite disorder (ASD) [295]. Generally, misplace of alternating corner shared BO_6 and $B'O_6$ octahedra from their ordered position leads to the ASD in DP crystal structure. Due to ASD, crystal possesses B-O-B or B′-O-B′ antisite coupling in place of B-O-B′ couplings [296]. Coexistence of antisite and spontaneous couplings in competing ferromagnetic (FM) and antiferromagnetic (AFM) interactions give rise to magnetic frustration that removes the FM long range ordering [296]. Moreover, the interface anisotropy between frustrated FM and AFM phase leads to EB effect [138]. Exchange bias is the phenomenon which associated with exchange anisotropy across the interfaces of ferromagnetic (FM) and antiferromagnetic (AFM), first noticed by Meiklejohn and Bean in 1956 in Co (FM) particles coated with a negative surface CoO (AFM) layer

[133]. A shift in the isothermal M (H) loop with respect to horizontal field axis and vertical magnetization axis is known as exchange bias effect [297]. When the magnetization is measured under field cooled (FC) and zero field cooled (ZFC) condition the corresponding effect known as conventional exchange bias (CEB) and spontaneous exchange bias (SEB) effect respectively. The M (H) loop shifts to the negative field directions and positive magnetization axis, known as negative EB effect. However, the reverse situation, namely, positive EB effect also occurs in some EB systems. Materials which show exchange bias effect can be applied for spin valve, permanent magnets, magnetic reading heads, ultrahigh-density magnetic recording and spintronics devices [298-300]. Additionally, along with the FM/AFM interface, EB effect has also been observed for FM/spin glass (SG), FM/ferrimagnetic (FiM), and AFM/SG interfaces. The doping of Sr^{+2} or Ca^{2+} in double perovskite in La^{+3} site enhance more interest because holes are doped into the compound. The doping of hole can effectively control the magnetic and electrical properties of lanthanide double perovskite [301]. In $La_{1.4}Ca_{0.6}CoMnO_6$ and $La_{1.6}Sr_{0.4}CoMnO_6$ perovskites some special magnetic properties were discovered [303, 304]. For a perfectly ordered system such as La_2CoMnO_6 (LCMO) valency of La, Co and Mn are +3, +2 and +4 respectively. In such systems, due to Co^{2+}-O-Mn^{4+} super-exchange interaction, the system shows perfect ferromagnetism (FM). Disorder at *B* sites leads to the possible Co^{3+} and Mn^{3+} states in LCMO and promotes AFM interactions [304].

Apart from EB, spin glass (SG) and cluster glass (CG) magnetic features have also been observed in DP oxide. Absence of long range order with frozen moment is the key factor for such glassy mechanism. When the disorder or frustration (competition between FFM/AFM components) is present in a small region of cluster at some freezing temperature (T_f), then it

is called as CG state. Whereas, SG state has appeared due to band disorder [289]. The atomic arrangement of B/B′ as Co/Fe i.e. A_2CoFeO_6 type DP structure has still unrevealed concepts. Because, Co/Fe based DP are less studied as compared to Co/Mn based DP. Fewer DPs like La_2CoFeO_6, Sr_2CoFeO_6, Pr_2CoFeO_6, $LaSrCoFeO_6$ have shown their interesting electrical and magnetic properties [68, 71, 72, 75]. Therefore, it is interesting and challenging to reveal the new content regarding the presence of divalent (Ca^{2+}) ion in La_2CoFeO_6 (LCFO) DP as LCFO shows a long range antiferromagnetic ordering at 270 K [68]. Thus, here, we report the effect of Ca^{2+} ion in electrical and magnetic properties of LCFO DP. In this report, we have presented $La_{1.5}Ca_{0.5}CoFeO_6$ (LCCFO) DP by solid state reaction method. Partial substitution of La^{3+} ion in LCFO by non magnetic Ca^{2+} ion enhanced the concentration of Fe^{4+} ions. Therefore, the FM Fe^{4+}-O-Co^{2+} (superexchange) and AFM Fe^{3+}-O-Co^{3+} (double-exchange) interactions are formed in the system. Present LCCFO system not only shows ferromagnetic long range ordering at T_C ~ 167 K but also exhibits short range two cluster regions (T_1 and T_S) at low temperature. In this material, giant EB has also been observed at 5 K.

6.2 Experimental details:

Polycrystalline sample of $La_{1.5}Ca_{0.5}CoFeO_6$ (LCCFO) was prepared by the solid state reaction in a conventional muffle furnace in air. High purity powders of La_2O_3, CoO, $CaCo_3$ and Fe_2O_3were taken in stoichiometric proportion, ground thoroughly and calcined in air at 1000 ^{0}C for 24 hours. Obtained powder re-ground and calcined again at 1250 ^{0}C for 24 hours. Thus obtained powder was pressed into the form of pellet and then sintered at 1350 ^{0}C for 36 hours and cooled to room temperature with cooling rate 50^{0}C/h. The crystal structure of polycrystalline sample is characterized by x-ray powder diffraction (XRD) technique with

Cu-Kα radiation (λ= 1.542 Å) at room temperature. The neutron diffraction measurements were carried out at the Dhruva reactor on a PD2 neutron powder diffractometer (λ=1.2443Å) in Bhabha Atomic Research Centre (BARC), Mumbai, India. X-ray photoemission spectroscopy (XPS) measurements were done using an Omicron multi probe surface analysis system with a monochromatic Al-Kα line at 1486.70eV and operating at an average base pressure of 9.7×10^{-11} Torr. The DC and AC magnetization measurements have been carried out using SQUID, superconducting quantum interference device based magnetic property measurement system (MPMS) in the temperature range of 2–300 K, with a maximum field of 7T.

6.3 Results and discussion:

6.3.1 Stability and Structure Analysis:

In order to assure the stability as well as to find out the crystal structure of DP, the value of tolerance factor (t) has been determined. For different crystal structure, the value of t varies differently [257]. For A-site doped DP i.e. $A_{2-x}A'_xBB'O_6$, t can be calculated by formula,

$$t = \frac{\left(1-\frac{x}{2}\right)r_A+\left(\frac{x}{2}\right)r_{A'}+r_O}{\sqrt{2}\left(\frac{r_B}{2}+\frac{r_{B'}}{2}+r_O\right)} \quad (6.1)$$

where, r_A, $r_{A'}$, r_B, $r_{B'}$ and r_O are shannon ionic radius of respective ions. The calculated value of t for LCCFO is 0.81, suggests monoclinic or orthorhombic crystal structure of LCCFO.

The phase purity, lattice parameters and approximate compositions of LCCFO sample is identified by XRD pattern which is recorded at room temperature. Fig. 6.1(a) shows the Rietveld refinement of XRD pattern of present compound obtained by Full-prof suite software. Absence of any impurity peak in XRD powder pattern of LCCFO confirms the

single phase and high purity of the sample. LCCFO material possesses monoclinic crystal symmetry structure with $P2_1/n$ (14) space group. As in comparison, the crystal structure of its parent compound

Cell Parameters	Value
a (Å)	5.467
b (Å)	5.432
c (Å)	7.689
α (°)	90
β (°)	89.973
γ (°)	90
V ($Å^3$)	228.373
Co-O1 (Å)	2.43252
Co-O2 (Å)	1.9612
Co-O3 (Å)	1.75086
Fe-O1 (Å)	1.83556
Fe-O2 (Å)	1.9041
Fe-O3 (Å)	2.17502
Co-O1-Fe (°)	158.599
Co-O2-Fe (°)	178.11
Co-O3-Fe (°)	170.395
χ^2	1.51

Table 6.1:- Structural parameters obtained by Rietveld profile refinement of the powder XRD pattern for $La_{1.5}Ca_{0.5}CoFeO_6$ at 300K. (Monoclinic – $P2_1/n$)

La_2CoFeO_6 (LCFO) possesses rhombohedral symmetry with R-3c space group at 300 K [68].

The fractional substitution of La site by Ca ion alters the crystal structure of LCCFO from rhombohedral to low symmetry monoclinic structure. Fig. 6.1(b) illustrates a polyhedral crystal structure of LCCFO obtained using VESTA software. In LCCFO structure, two octahedra (FeO_6 and CoO_6) are not located alternatively on the cubic edge and create the system as an anti-site disordered system [289]. All the grabbed structural parameters from Rietveld refinement are listed in table 6.1. It can be seen from the table 6.1 that the bond

angles and bond lengths of system are not identical i.e. Fe/Co-O-Co/Fe≠180° and Fe-O≠ Co-O. Hence, it is clear from all the refined parameters and fig.6.1(b) that LCCFO system has distorted crystal structure. These bond angles and bond lengths are also not same as bond angles and bond lengths of ordered DP [305]. Therefore, addition of divalent ion in LCFO changes the crystal structure. Consequently, the disorder in LCCFO crystal structure affects the physical and magnetic properties like in other perovskite [296].

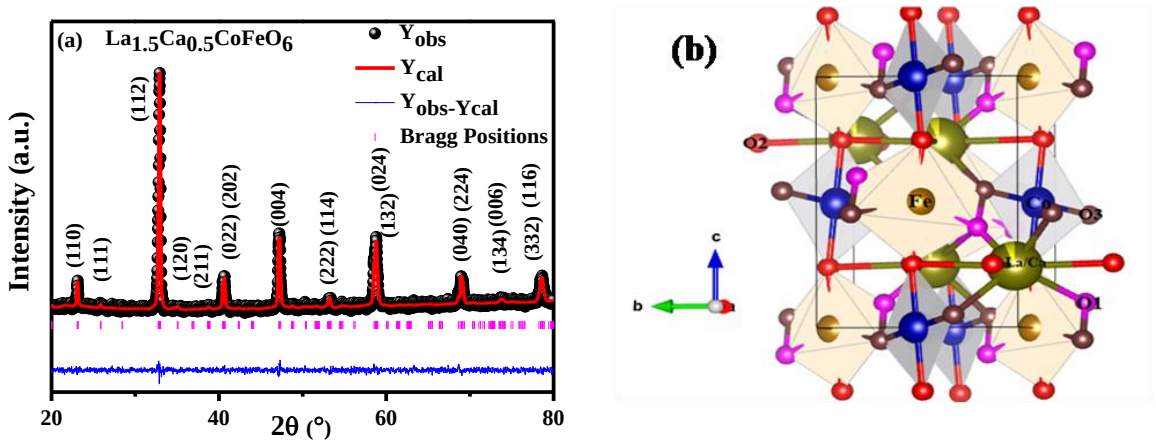

Figure 6.1(a) The XRD pattern along with the Rietveld refinement of LCCFO at 300 K. **(b)** The Crystal structure of LCCFO sample using VESTA.

6.3.2 X-ray photoelectron spectroscopy (XPS) Analysis:

All the physical and magnetic properties of sample are highly influenced by chemical electronic states of its each constituent. Therefore, to analyze the surface electronic state of elements in LCCFO, the core level XPS technique has been performed as shown in fig. 6.2. All the physical and magnetic properties of sample are highly influenced by chemical electronic states of its each constituent. The peak positions and doublet separations of the recorded XPS data displayed in fig. 6.2 have been decided from the National Institute of Standard and Technology (NIST) XPS database [306]. Herein, fig. 6.2(a) shows the full surface scan spectrum and confirms the existence of La, Ca, Co, Fe and O in LCCFO sample.

Along with these ions, C 1s (carbon) peak at 284.24 eV is also present in sample. This C 1s peak is attributed to residual carbon which is absorbed from air at the surface of sample. The separately collected XPS spectra of individual elements are shown in fig. 6.2 (b-f). All XPS peaks were fitted by XPSPEAK4.1 software. Fig. 6.2 (b) shows the La 3d core-level XPS spectra as split into two La $3d_{5/2}$ and La $3d_{3/2}$ peaks due to spin orbit coupling. Every peak further deconvoluted into two peaks. These two peaks are emerged due to the occupancy of La 4f state into $4f^0$ and $4f^1$ states in the final state of core hole [307]. The two doublet peaks of La are observed with doublet separation approximately 16.9 eV which is corresponds to La^{3+} valance states [308]. Fig. 6.2 (c) displays the XPS result of the Ca 2p core-level spectra at $2p_{3/2}$ and $2p_{1/2}$ of the LCCFO sample. From XPS result, it is found that calcium exists in divalent state in LCCFO with binding energy 346.7 eV ($2p_{3/2}$), 350.3 eV ($2p_{1/2}$) with doublet separation of 3.6 eV for Ca^{2+} [309].

The XPS spectra of compounds which contain Co ions are highly interesting. As, Co core level spectra exhibits not only photoelectrons lines but also shows shake-up satellite peaks which are sensitive to oxidation states as well as ligand co-ordination [70, 310, 311]. The 2p core level spectrum of Co in LCCFO has been shown in fig. 6.2 (d). Due to spin orbit split, the separation (ΔE) of Co $2p_{1/2}$ and Co $2p_{3/2}$ peaks is ~15.5 eV. The same Co 2p peak separation in Co_3O_4 (mixed +2 and +3 state) and in CoO (+2 state) are reported to be 15.3 eV and 15.9 eV respectively. Thus, for LCCFO sample, the Co ion possesses mixed +2/+3 states. The presence of two charge transfer satellite ~ 7 eV above Co 2p main peaks confirms the divalent state of Co ion in present sample [310, 311]. Therefore, the presence of these weak satellite peaks discarded the existence of only Co^{3+} ion. Because, compounds containing Co ion in +3 oxidation state like Co_2O_3 either do not show these satellite peaks or

shows less intense peaks. In our case, Co spectra shows these satellite peaks like Co_3O_4 compound, which confirms the mixed $Co^{2+/}Co^{3+}$ valance sates [311, 312]. Consequently, the calculated relative concentration of Co^{2+} and Co^{3+} states is about 58% and 42% respectively. Fig. 6.2(e) shows the fitted core-level spectrum results of Fe 2p for the LCCFO sample. Fe 2p XPS spectra show a doublet of $2p_{3/2}$ and $2p_{1/2}$ excitation due to spin-orbit splitting. The peaks appear at binding energy 710.0 and 712.8 eV correspond to Fe^{3+} ($2p_{3/2}$) and Fe^{4+} ($2p_{3/2}$) respectively, and the peaks at 723.0 and 725.8 eV correspond to Fe^{3+} ($2p_{1/2}$) and Fe^{4+} ($2p_{1/2}$), respectively [312]. The satellite peak around 718.1 eV can be assigned to the Fe^{3+} species. These values are consistent with those reported by Ghaffari et al. [313]. The calculated relative concentration of Fe^{3+} and Fe^{4+} states are about 55% and 45% respectively. Fig. 6.2(f) shows the O 1s core level spectra. In this spectrum, two peaks are appearing at 528.4 eV and 531.2 eV binding energies. The peak around ~ 528.4 eV corresponds to O^{2-} ions of lattice oxygen [138], whereas the other peak around 531.2 eV is probably due to hydroxyl groups and carbonate compounds which are adsorbed at the surface of sample [314].

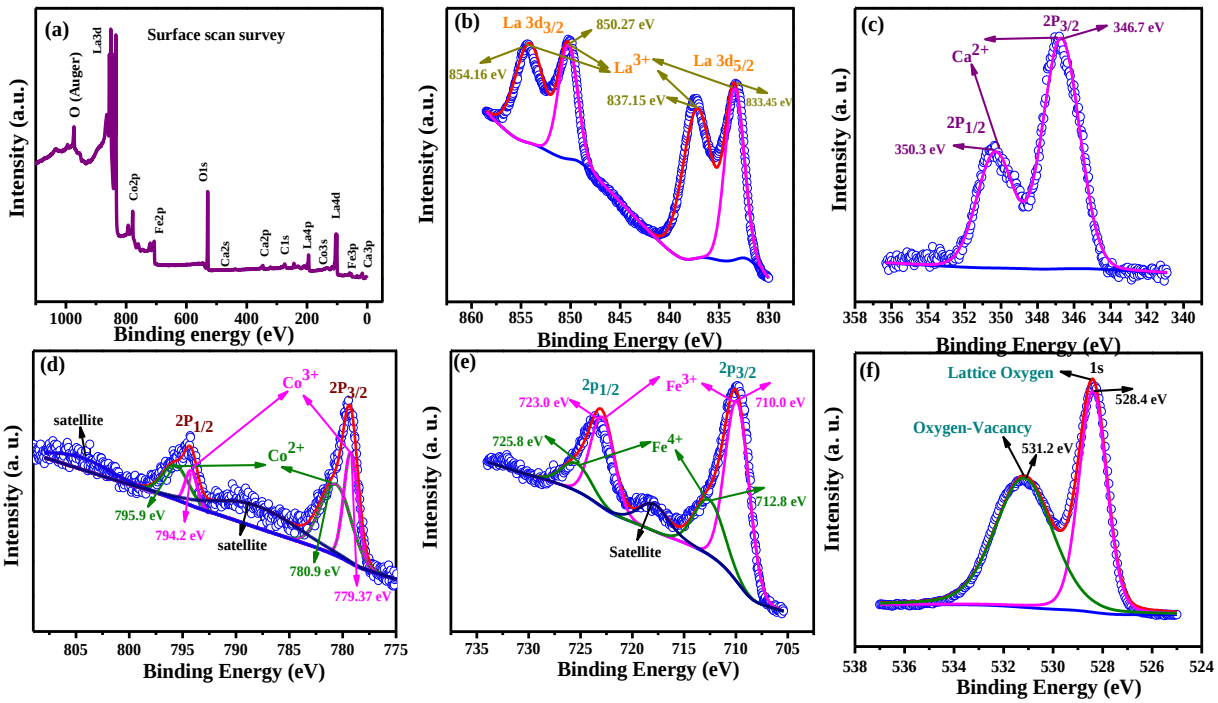

Figure 6.2(a): The full XPS surface scan survey of LCCFO sample. Deconvoluted XPS Spectra of LCCFO **(b)** La 3d level, **(c)** Ca 2p level, **(d)** Co 2p level, **(e)** Fe 2p level and **(f)** O1s level.

6.3.3 Theoretical Analysis :

We have performed the *ab* initio calculations based on density function theory (DFT) using Vienna *ab* initio simulation package (VASP) [133]. Exchange-correlation potential (Perdew-Burke-Ernzerhof exchange-correlation functional) is approximated with generalized gradient approximation (GGA) [315]. The projector augmented wave method (PAW) is used for core-valence interaction. The Self Consistent Field (SCF) convergence is done with 3×3×2 K-mesh griding and 400 eV Plane-wave cut off energy. Consequence Spin Polarized Density of State (SPDOS) is done 5×5×4 K-mesh griding (using NEDOS = 1000).

To calculate the spin polarized partial and total DOS, we have considered the on-site coulomb correction (GGA+U). The Hubbard U corrections are considered to be ~3 eV for La-4f states, ~3 eV for Ca-3p states, ~3 eV for Co-3d states and ~4 eV for Fe-3d states [71].

Calculations were performed both for FM and AFM couplings among spins. Ground state energy of the FM configuration is -67.86 eV per formula unit and ground state energy of AFM configuration is – 67.80 eV. Although FM configuration is slightly energetically favourable, the magnitude of the ground state energies for both FM and AFM are almost same indicating the mixed state behavior. This mixed magnetic state may be associated to ferrimagnetic ground state. The total density of states (TDOS) of LCCFO (fig. 6.3a) for the FM and AFM interactions is observed carefully. The absence of any states near Fermi level suggests an insulating nature of the system. Moreover, it was observed that La-*f*, Co-*d*, Fe-*d* and O-*p* states (fig. 6.3 b) have the dominant contribution in their respective spin integrated partial density of states PDOS. These PDOS curves show strong hybridization among O-p and Co/Fe-d sates. The large asymmetry was observed in the PDOS of both B and B' site ion (i.e. Co-d and Fe-d respectively) as shown in (i) and (ii) inset of fig. 6.3 b. This spin polarized asymmetric behaviour of Co and Fe ion suggests their magnetic nature in LCCFO system.

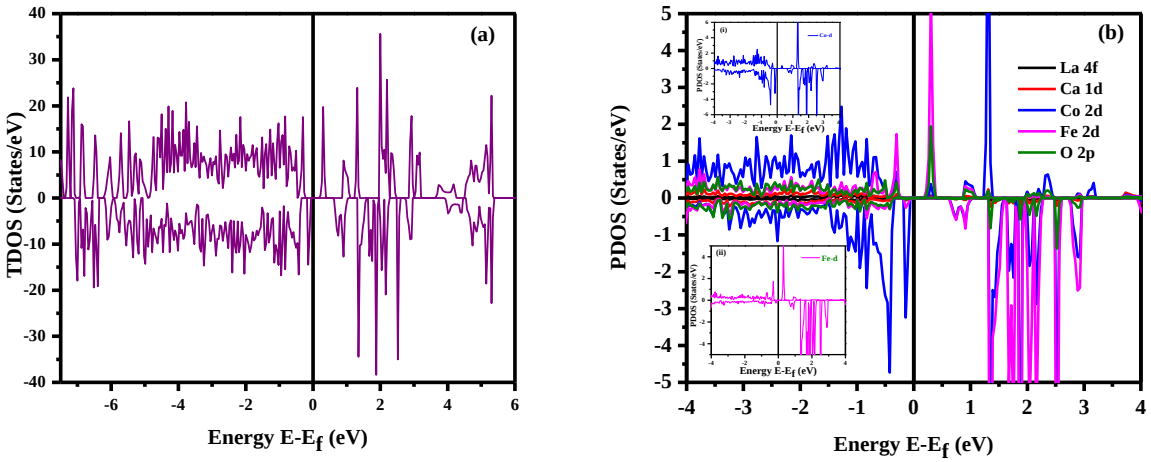

Figure 6.3(a) : TDOS of LCCFO system. **(b):** Spin resolved PDOS for La-f, Ca-d, Co-d, Fe-d, and O-p orbitals inset **(i)** PDOS of Co-d state. **(ii)** PDOS of Fe-d state.

Top of the valence band lies at 10 meV below the Fermi level and bottom of the conduction band lies at 38 meV above the Fermi level. This band gap between the valence and conduction band confirms the insulating behaviour of present system.

6.3.4 Temperature dependent Neutron diffraction Analysis:

As the Fe and Co ions have possesses comparable X- ray atomic structure factors, so it is impossible to evaluate the accurate crystal structure from the XRD data only. As a matter of fact, in order to find the magnetic structure and to confirm the antisite disorder in LCCFO system, we have performed temperature dependent neutron powder diffraction (NPD) experiment. Fig.6.4a shows the Rietveld refined neutron diffraction patterns at various temperatures (6 K to 300 K). All the NPD patterns have been refined with the nuclear monoclinic structure (P21/n space group). From fig.6.4a, it is evident that Bragg peak at ~16^0 is not present in room temperature NPD pattern. But, on lowering the temperature from 300 K i.e. below 200 K, a super lattice reflection peak (011) is appeared. This reflection peak has attributed to magnetic ordering or contribution from magnetic phase P-1. Thus, this super-lattice reflection peak at 6 K, 15 K, 30 K, 50 K, 100 K, 150 K is the clear indication of presence of magnetic ordering in LCCFO system. This is also consistent with our magnetic analysis. Further, this NPD refinement confirms the presence of antisite disorder at B-site. Around 28% of antisite disorder is present in LCCFO system. We have also extracted the values of magnetic moment of Co and Fe sub-lattices which reside at Wyckoff positions of 2d and 2c respectively. The temperature dependent values of magnetic moments of Fe and Co sub-lattices are listed in table 6.2. From this magnetic moment value and from its magnetic spin structure (fig. 6.4b) which is derived from 6 K NPD data, it is clear that

LCCFO system possesses ferrimagnetic ground state below 200 K. The DFT study also revealed the ferrimagnetic ground state of LCCFO system. The similar ferrimagnetic ground state has been reported in $Al_{0.5}Ga_{0.5}FeO_3$ and $FeMnO_3$ [316, 317].

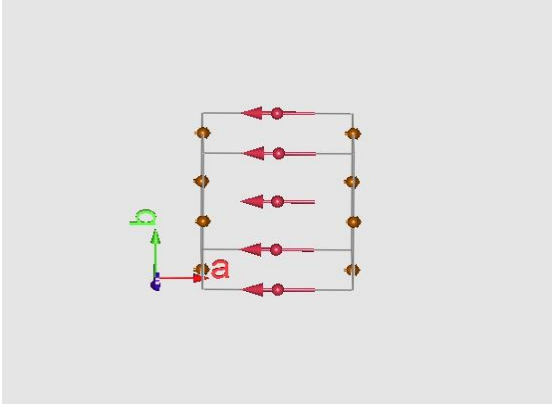

Figure 6.4 (b): Magnetic structure of LCCFO from 6 K NPD data.

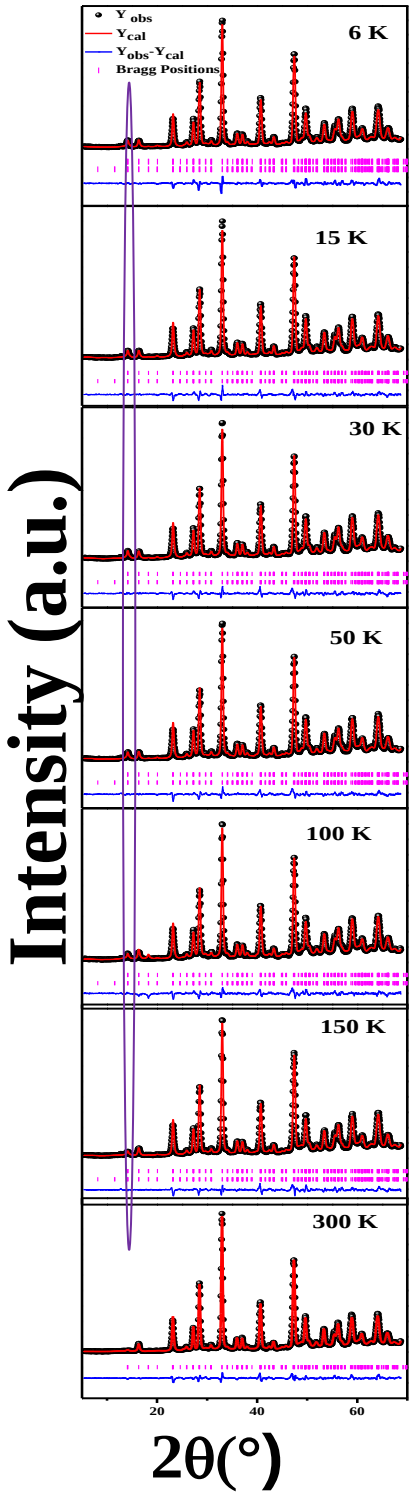

Figure 6.4 (a): Rietveld refined neutron diffraction patterns at various temperatures of LCCFO system. The oval marked area indicates the purely magnetic (011) Bragg peak.

Temperature	Magnetic moment (μ_B) of Fe sub lattice	Magnetic moment (μ_B) of Co sub lattice
6 K	0.59	-2.705
15 K	1.162	-2.046
30 K	1.207	-2.158
50 K	1.612	-1.481
100 K	1.653	-0.942
150 K	0.863	-1.235
300 K	0.002	-0.002

Table 6.2:- The magnetic moment values of Co and Fe sublattices evaluated by NPD data at different temperatures.

6.3.5 Magnetic Analysis:

In previous study of LCFO DP, only two transitions were observed from its magnetic study. A magnetic phase transition at T_N ~ 270 K and a structural change anomaly around T ~ 200 K [68]. In order to glance the effect of divalent cation (Ca^{2+}) in LCFO, we have carried out the DC and AC magnetization measurement of LCCFO sample. Fig. 6.5(a) shows the temperature dependent magnetization (M-T) graph of present system at 100 Oe magnetic field under zero field cooling (ZFC) and field cooling (FC) protocol. Here, a paramagnetic (PM) to ferrimagnetic (FiM) transition is occurred at T_C ~ 167 K. NPD analysis also confirms the presence of magnetic ordering below 200 K. There is also a bifurcation between ZFC and FC curves below 120 K which signifies the presence of spin frustration or some type of glassy state [318]. Two magnetic phase transitions (T_1 ~ 11 K and T_C ~ 167 K) scenario can be seen in dM/dT Vs T curve (inset of fig. 6.5a) of LCCFO for 100 Oe FC curve. The transition corresponding T_C has been assigned to the magnetic exchange interaction between Co^{2+}/Co^{3+} and Fe^{3+}/Fe^{4+} via O^{2-} as $(Co/Fe)^{3+}$-O^{2-}-$(Fe/Co)^{3+}$ or Co^{2+}-O^{2-}-Fe^{4+} [138]. A change in the slope can also be seen below 10 K in magnetic moment (fig.

6.3a). This transition is pronounced as a peak in M-T graph on application of magnetic field > 100 Oe (fig. 6.5b). This may be assigned for canted antiferromagnetic (CAF) phase transition below 10 K [319]. Moreover, strange behaviour has been observed in its ZFC M-T curves for different applied magnetic field as shown in fig. 6.5b. Three major facts have been highlighted in same M-T curve. (i) Significant change in magnetization value below T_C i.e. rise of a sudden cusp for applied H > 100 Oe. (ii) On applying a higher magnetic field H = 1000 Oe and 10000 Oe, the magnetization suddenly drops at low temperature. (iii) The T_C values shifted towards low temperature with increases in the strength of magnetic field. A foresaid unusual nature of M-T graph can be understood by the presence of compelling mechanism at low temperature. First one, the existence of another magnetic phase such as AFM components along with FM components i.e. the presence of spin frustration. The reduction in magnetization value can be manifested by super exchange interactions between Co^{2+}/Co^{3+}-O^{2-}-Co^{2+}/Co^{3+} and Fe^{3+}/Fe^{4+}-O^{2-}-Fe^{3+}/Fe^{4+} [289]. This AFM nature can also be associated with 4d-3d [La^{3+}-Co^{2+}/Fe^{4+}] negative exchange interactions [320]. M-H curves at very low temperature also prove the dominant AFM nature in LCCFO which is shown in fig. 6.7a. Second one, the formation of antiphase boundaries (APBs) due to presence of antisite disorder in system. These types of planar defects are also observed in Y_2CoMnO_6 DP, La_2CoMnO_6 thin films [321, 322]. At the APB-domain borders, interaction between atoms leads to strongly pinned magnetic domain walls. At this case, Co-O-Co or Fe-O-Fe interactions across the APB will change the orientation of neighboring Co/Fe interacted FM domains in antiparallel direction. This process could lead to decrease in magnetization value [323].

Further, to estimate the effective paramagnetic momemt (μ_{eff}) and Curie-Weiss temperature (θ_{CW}) of LCCFO, we have performed the Curies-Weiss (CW) fit at the experimental (χ^{-1} Vs T) curve of 1000 Oe ZFC data in the paramagnetic region. The CW law is stated as

$$\chi^{-1} = \frac{T}{C} - \frac{\theta_{CW}}{C} \quad (6.2)$$

The CW fit is shown in inset of fig. 6.5c. The yielded experimental values of θ_{CW} and μ_{eff} are 96.51 K and 3.729 μ_B respectively. Although, there is a large difference between the θ_{CW} and T_C values which further confirms the spin frustration in the system. The experimentally obtained effective spin only moment from CW fit is comparatively matches with the theoretical spin only moment value μ_{eff} = 3.739 μ_B. For theoretical spin only moment calculation, we have considered the spin state of Co and Fe ion as Co^{2+}: high spin state (S=1/2), Co^{3+} : low spin state (S=0), Fe^{3+} : low spin state (S=1/2), Fe^{4+} : high spin state (S=1).The magnetic feature of Co and Fe ions are also confirmed from theoretical and neutron diffraction study.

One more riveting magnetic phenomenon has appeared in temperature variation of inverse susceptibility curve. In inset of fig. 6.5c, it can be seen that there is a violation of CW law. A down turn deviation from the expected linear behaviour of PM state at above the T_C ~ 167 K. This down turn type of behaviour is commonly known as Griffith phase (GP). Particular in this region, system neither behaves as a PM nor acts like FM/AFM [21, 324, 325]. To ensure GP regime, we have fitted our inverse susceptibility data by power law which is given by,

$$\chi^{-1}(T) \propto (T - T_c^R)^{1-\lambda} \quad (6.3)$$

where, λ (0<λ<1), a power law exponent is the measure of deviation from FM [324, 325]. Generally, the power law is fit for the values of $T_c^R \approx T_C$. However, in LCCFO system, due to frustration, there is a large difference between T_C and θ_{CW} values i.e. $\theta_{CW} << T_C$. In this situation, it is always better to choose $T_c^R = T_C$ [326]. Thus, the $\log_{10}(1/\chi)$ Vs. $\log_{10}(T\text{-}T_c^R)$ plot of 1000 Oe ZFC experimental data along with power law fit has been shown in fig. 6.5c . The obtained value of λ from fit is 0.015. The presence of short range correlated clusters in GP regime may be associated with the antisite disorder (ASD) [327]. However, futher experimental verification is needed for GP.

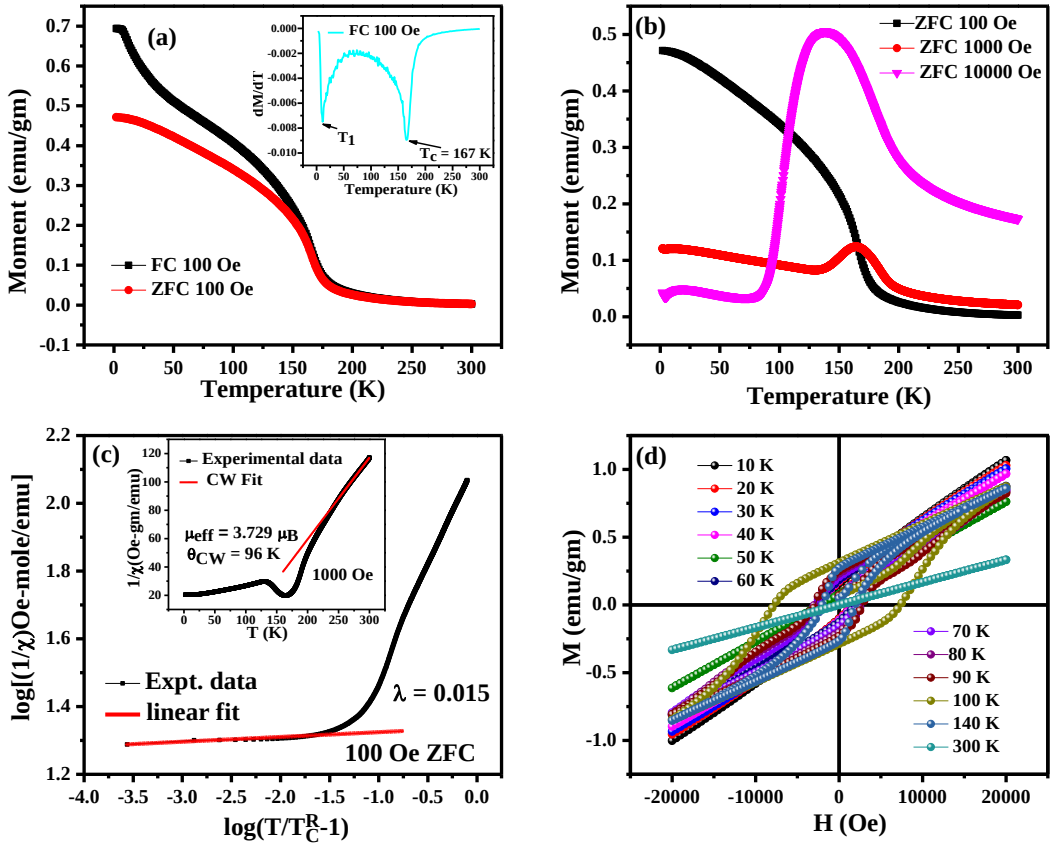

Figure 6.5(a) : ZFC and FC curve of LCCFO sample at 100 Oe magnetic field. **Inset** : Temperature dependence of dM/dT for FC data at 100 Oe magnetic field. **(b)** Temperature dependence of the magnetization under ZFC protocol at H = 100 Oe, 1000 Oe and 10000 Oe**. (c):** Power-law fitting to the log-log plot of "$1/\chi$ Vs $((T\text{-}T_C^R)/T_C^R)$ at 100 Oe ZFC data. **Inset**

: Inverse susceptibility Vs temperature curve at 1000 Oe magnetic field with Curie-Weiss law fit. **(d):** M(H) curves of LCCFO at different temperature.

As shown in fig. 6.5a, a bifurcation observed between ZFC and FC data at 100 Oe field implies the presence of frustration at low temperature. Thus, to reveal the essence of magnetic frustration and to ensure glassy nature in magnetic system, we have characterized our sample by AC magnetic susceptibility technique in presence of zero magnetic field. Three transitions are observed in χ_{AC} measurement, first are at T_C ~167 K, second are at T_1 ~ 11 K and third is at T_S ~ 35 K. The first observed peak in $\chi'(T)$ and $\chi''(T)$ {fig. 6.6a} at T_C ~167 K does not show any frequency dependency i.e. this sharp transition can be attributed to long range FM ordering due to Co^{2+}-O^{2-}-Fe^{4+} or Co^{3+}-O^{2-}-Fe^{3+}interactions. The frequency independent nature unlike first transition peak is not common for second and third transition peaks. In fact, both T_1 and T_S peaks are exhibiting a clear shift by varying applied frequency. In this way, two glassy phase like phenomenon has appeared in $\chi'(T)$ and $\chi''(T)$curves from T = 2 to 50 K {fig. 6.6b}. To confirm the spin glass (SG)/cluster glass (CG) like nature in LCCFO, the dynamic scaling law (DSL) fit and Vogel fulcher (VF) fit at T_1 and T_S have been carried out. The equation for DSL fit [124, 126] is

$$f = f_0 \left(\frac{T_f - T_{SG}}{T_{SG}}\right)^{z\nu} \tag{6.4}$$

where, T_{SG} is spin glass (SG) freezing temperature, $\tau_0$is spin flipping time $(\tau_0) = \frac{1}{f_o}$ and zν is the dynamical critical exponent. Whereas, VF law [129] is given as

$$f = f_0 \exp\left(-\frac{E_A}{K_B(T_f - T_0)}\right) \tag{6.5}$$

where, T_o is VF temperature or inter cluster interaction strength and E_A is activation energy. DSL and VF fit along with experimental data at temperatures T_1 is shown in fig 6.6c and inset of fig. 6.6c respectively. Whereas, DSL and VF fit along with experimental data at

temperatures T_S is shown in fig.6.6d and inset of fig. 6.6d respectively. The main parameters yielded by both fittings are displayed in table 6.3.

Parameter	**T_1 (K)**	**T_S (K)**
Mydosh Paramter	p = 0.108	p = 0.198
Dynamic Scaling law	Zv= 4.32 $\tau_0 = 2.325 \times 10^{-5}$ sec T_{SG} = 12. 66 K	Zv= 0.74 $\tau_0 = 3.84 \times 10^{-4}$ sec T_{SG} = 36.30 K
Vogel fulcher fit	T_0 = 10.243 K $\tau = 3.6 \times 10^{-5}$sec	T_0 = 34.18 K $\tau = 6.25 \times 10^{-4}$sec

Table 6.3:- Fitted parameters obtained by dynamic scaling law and Vogel fulcher fit at T_1 and T_S temperatures.

The obtained values of characteristics relaxation time (τ) for transition T_1 and T_S are ~10^{-5} sec and ~10^{-4} sec respectively. The spin flipping time for both low temperature transitions is quite larger than the $\tau_0$value for typical spin glass (10^{-12}-10^{-13} sec). Thus, the T_1 and T_S both transitions are considered to show reentrant cluster glass (RCG) behaviour. Higher τ_0 values and low Zv values implies that both relaxation process in LCFFO are slower and indicate the presence of randomly oriented spin clusters [328, 329].

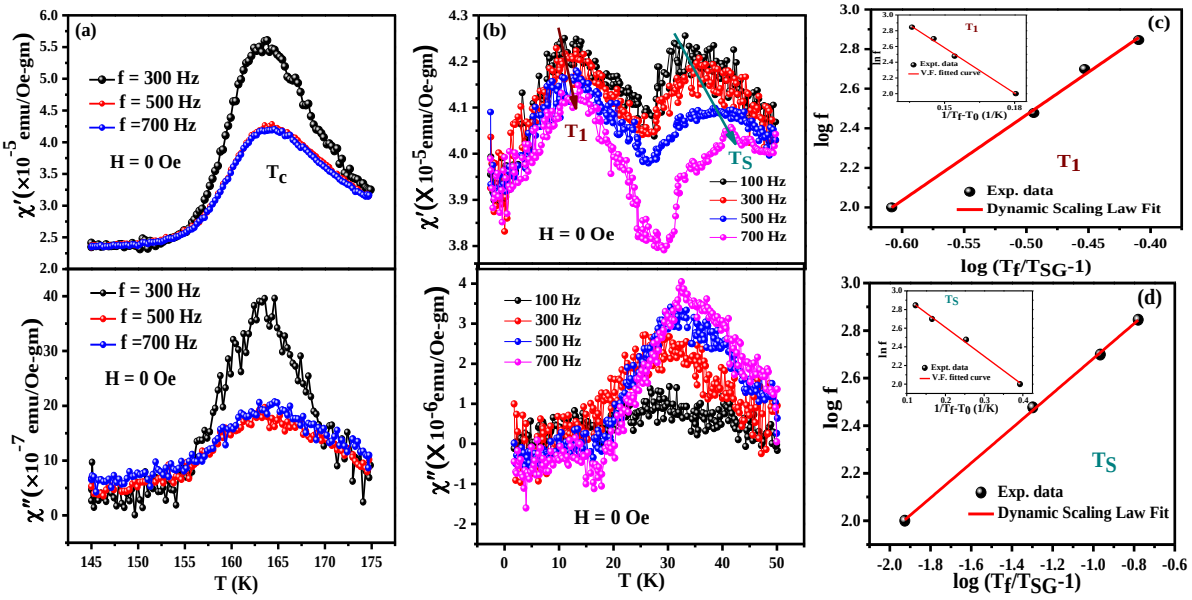

Figure 6.6: Temperature dependence of the AC susceptibility of LCCFO at zero magnetic field. **(a)Upper panel :** The real part χ' and **lower panel** : The imaginary part χ'' from T = 140-180 K. **(b)Upper panel :** The real part χ' and **lower panel** : The imaginary part χ'' from T = 2-50 K. T_1 and T_s are the cluster glass temperature. **(c)** Dynamic Scaling fit of log f Vs log (T_f/T_{SG} -1) curve. **Inset** : Vogel-fulcher fit ln *f* Vs $1/(T_f-T_o)$ data in the T_1 RCG region. **(d)** Dynamic Scaling fit of log f Vs log (T_f/T_{SG} -1) curve. **Inset** : Vogel-fulcher fit of ln *f* Vs $1/(T_f-T_o)$ data in the T_S RCG region.

Moreover, Mydosh parameter (p) also defines the types of glassy phase [122]. It can be calculated as

$$p = \frac{\Delta T_f}{T_f \Delta \log_{10}(f)} \tag{6.6}$$

The values of p are generally found in range 0.004-0.018 for SG process and for super paramagnets, p lies in between 0.3-0.5. While, for CG state, the p values lies between SG and super paramagnets values [122, 330]. Again, the calculated value of p (table 6.3) for both T_1 and T_S are stand for RCG.

The origin of both spin clusters at low temperature (T_1 and T_S) can be associated with local magnetic frustration and site-antisite disorder. The competition between both AFM interactions (Co^{2+}-O^{2-}-Co^{2+}/ Fe^{4+}-O^{2-}-Fe^{4+}/ Co^{3+}-O^{2-}-Co^{3+}/ Fe^{4+}-O^{2-}-Fe^{4+}) and FM

interactions (Co^{2+}-O^{2-}-Fe^{4+}/ Co^{3+}-O^{2-}-Fe^{3+}) causes the local magnetic frustration at the antiphase interface. Therefore, the driving spin clusters get slowed down and do not obey time dependent AC fields. Hence, system shows CG like relaxation process. In conclusion, there are the formations of two types of magnetic spin clusters in LCCFO due to the presence of antisite defects. First (I) Cluster (at T_1~11 K) is due to coexistence of FM interactions (Co^{3+}-$O^{2-}$$Fe^{3+}$) and AFM interactions ($Co^{3+}$-$O^{2-}$$Co^{3+}$/ Fe^{3+}-O^{2-}-Fe^{3+}). Second (II) Cluster (at T_S~35 K) is due to coexistence of FM interactions (Co^{2+}-O^{2-}-Fe^{4+}) and short range AFM interactions (Co^{2+}-$O^{2-}$$Co^{2+}$/ Fe^{3+}-O^{2-}-Fe^{3+}). It is assumed that II cluster has larger volume as compared to the cluster I due to low volume fraction of anion defect region. Thus, II (T_S) cluster freezes at high temperature relative to I cluster (T_1) [331]. In contrast to LCCFO, $LaSrCoFeO_6$ (LSCFO) shows a single SG relaxation at 72 K [75].

Since, LCCFO system has the low temperature magnetic competition between FM and AFM components. Therefore, we have further explored the exchange bias (EB) effect. Fig. 6.5d depicts the ZFC M-H curves of LCCFO at different temperatures. From this figure, it is clear that present material exhibits the PM nature at 300 K. As we decrease the temperature and measured the M (H) loop below the T_c ~167 K the squareness in M (H) loop is appeared (140 K) and it is decreasing as decrease in temperature, which again confirms the AFM phase is dominating at low temperature. Below 100 K, the M (H) loop is shifted toward the negative magnetic axis and positive magnetization axis which is mainly due to the exchange bias effect. Both spontaneous exchange bias (SEB) as well as conventional exchange bias (CEB) effect has been observed at low temperature for LCCFO. The EB field (H_{EB}) and coercivity (H_C) are defined as $H_{EB} = (H_L + H_R)/2$ and $H_C = (|H_L| + |H_R|)/2$, respectively, where H_L and H_R are the left and right coercive field. The EB Magnetization (M_{EB}) and

remanent magnetization (M_R) are defined as $M_{EB} = (H_{R1} + H_{R2})/2$ and $M_R = (|M_{R1}| + |H_{R2}|)/2$, respectively, where M_{R1} and M_{R2} are the two intercepts of magnetization axis [138, 332-333].The vertical and horizontal shifts in M-H curves may also occur due to unsaturated minor loop effect [334]. Therefore, to rule out such effect for LCCFO, we have measured M-H loop at 5 K by cooling the system in both ±50 kOe magnetic fields. Fig. 6.7b shows that under -50 kOe cooling filed, M-H loop shifted towards the negative side of the H axis, while for+ 50 kOe cooling filed it was shifted towards positive side of H axis. Thus, this observation discarded the possibility of an unsaturated minor loop effect [335].

Due to interesting nature of M(H) curves at different temperatures, we have analyzed the M(H) data in four temperature regions. **(a)** Fig.6.7a shows the M-H curve at 5 K with ±70 k Oe magnetic field which supports the dominant AFM component in system as magnetic moment did not saturate up to such a high applied magnetic field. Moreover, this ZFC M(H) curve is totally shifted in negative field axis and in positive magnetization axis. Due to this asymmetric nature, M(H) loop of LCCFO at 5 K exhibits SEB effect. The values of H_{EB} and M_{EB} are 2.106 k Oe and 0.083 emu/gm respectively. The CEB effect has also investigated at same temperature in FC condition. Sample was cooled in ± 5T magnetic field and M (H) loops were measured at 5K, we got large CEB effect in LCCFO sample. There are large shift in M (H) loops from origin as shown in the fig. 6.7b.

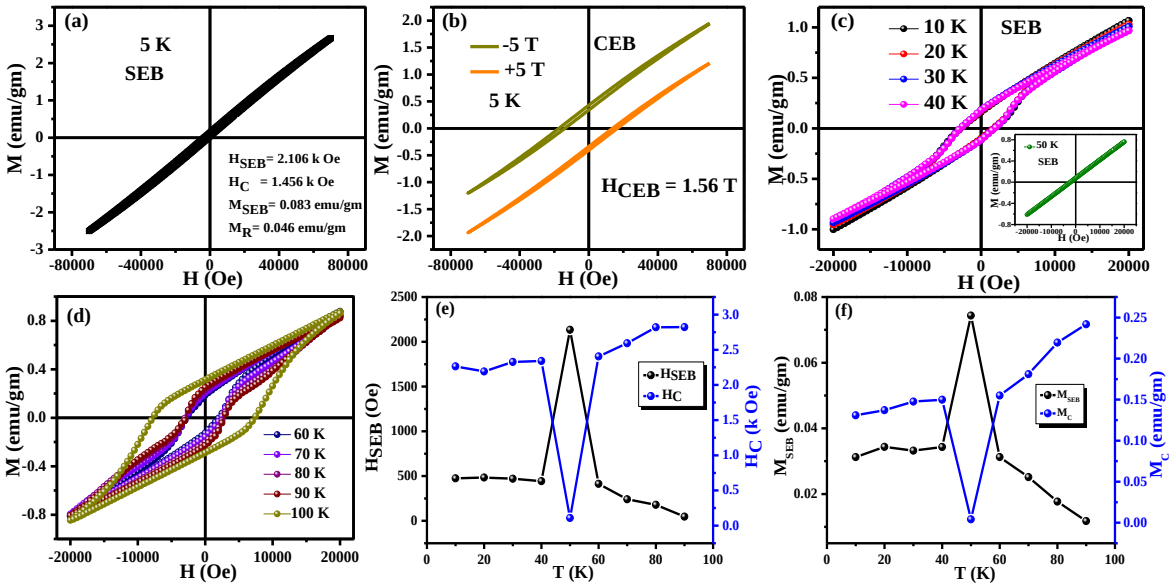

Figure 6.7(a) : ZFC M(H) isotherms in the range ±70 kOe at 5 K. **(b)** The M(H) isotherms measured at 5 K after cooling the sample under +50 kOe (green curve) and −50 kOe (orange curve). **(c):** ZFC M(H) isotherms in the range ± 20 kOe at 10 K, 20 K, 30 K and 40 K. **Inset :** ZFC M(H) isotherms in the range ± 20 kOe at 50 K **(d):** ZFC M(H) isotherms in the range ± 20 kOe at 60 K, 70 K, 80 K, 90 K and 100 K. **(e):** Variation of H_{EB} (left Y –axis) and H_C (right Y-axis) with the temperature (10 – 90 K). **(f):** Variation of M_{SEB} (left Y –axis) and M_C (right Y-axis) with the temperature (10 – 90 K).

When sample was cooled to 5K at +5T magnetic field in FC mode, a large shift in M(H) has been observed toward negative field axis and positive magnetization axis which assigned for CEB effect. Similarly field cooling was done for – 5T magnetic field and again M (H) loop measured at 5K then same amount of shift was observed in opposite direction i.e. positive field axis and negative magnetization axis as shown in the fig. 6.7b. The shift in M (H) loops for maximum positive and negative field are almost the same, which is further indicating that this loop shift is not due to a minor loop effect [336]. The shift in M (H) loops under FC condition called CEB field (H_{CEB}) has a giant value (H_{CEB} ~1.5T). Due to additional unidirectional anisotropy after FC, there is a large shift in FC MH loop [5]. **(b)** (10- 40 K), the ZFC M(H) loop of this temperature region also shows SEB. Prominent hysteresis loop for this T range confirm the significant FM components along with AFM

component as loop is not saturated upto ± 20 k Oe magnetic field {fig. 6.7c}. **(c)** At 50 K, again the astonishing nature of curve has been appeared. A sudden sharp shoot up was observed in SEB value of system at 50 K (inset of fig. 6.7c). From inset of fig. 6.7c, it is clear that ZFC M(H) loop at 50 K also totally shifts in negative magnetic axis. This nature may be associated with the cluster glass relaxation phenomenon. Because, below this temperature, type II magnetic cluster start to freeze. Thus, at this interface, there is a strong competition between FM and AFM matrix. **(d)** (60- 100 K), The SEB effect exists upto 90 K. At 100 K, a prominent, large, significant but symmetric hysteresis loop conveys the presence of strong FM interactions in the system (fig. 6.7d). We have also shown the variation of values of H_{EB}, H_C, M_{EB} and M_R with the temperature (10 – 90 K) in fig. 6.7e and fig. 6.7f.

In this way, we inferred that present system LCCFO has multiple magnetic phases like FM/AFM/CG. Both DC and AC magnetic study is the evident of different phase separation of this system. From XPS study, it is confirmed that doping of Ca^{2+} ion at La^{3+} site changes the valance states of Co and Fe ions and they vary in two configurations as [Co^{2+}-Fe^{4+}] and [Co^{3+}-Fe^{3+}]. Due to this, various FM and AFM couplings are generated. Misallocation of transition 3d metal ions from their real positions also a reason of AFM interaction. Thus, there are Co-O-Co or Fe-O-Fe interactions in CoO_6 or FeO_6 octahedron due to the presence of ASD. Hence, CAF anisotropy at low temperature and coexistence of FM/AFM/CG phase are the possible reason of observed SEB and CEB effect [138].

6.4 Conclusion:

We have presented the structural and magnetic properties of $La_{1.5}Ca_{0.5}CoFeO_6$ system. The LCCFO system shows ferromagnetic transition (T_C ~ 167 K). The ferromagnetic ground

state is also confirmed by DFT and neutron powder diffraction. Low temperature double re-entrant cluster glass transitions (T_1~ 11 K and T_S~35 K) are observed which has been attributed to the presence of ASD effect. It is also observed that the present system consists of large H_{SEB} ~ 2.106 kOe and giant H_{CEB} ~ 1.56 T at 5 K. SEB effect in LCCFO system persists up to 90 K. The presence of double cluster glass, large EB effect and different magnetic phases make this LCCFO system a strong candidate for spintronics devices.